Supplementary Materials for

Decoding motor imagery from the posterior parietal cortex of a tetraplegic human

Tyson Aflalo, Spencer Kellis, Christian Klaes, Brian Lee, Ying Shi, Kelsie Pejsa, Kathleen Shanfield, Stephanie Hayes-Jackson, Mindy Aisen, Christi Heck, Charles Liu, Richard A. Andersen*

*Corresponding author. E-mail: andersen@vis.caltech.edu

Published 22 May 2015, *Science* **348**, 906 (2015)
DOI: 10.1126/science.aaa5417

This PDF file includes:

Other Supporting Online Material for this manuscript includes the following:
(available at www.sciencemag.org/content/348/6237/906/suppl/DC1)

Supplementary Materials:

Materials and Methods

Figures S1-S3

Movies S1-S3

References (23-26)

Materials and Methods:

All procedures were approved by the California Institute of Technology, University of Southern California, and Rancho Los Amigos Internal Review Boards. Informed consent was obtained from EGS after the nature of the study and possible risks were explained. Study sessions occurred at Rancho Los Amigos National Rehabilitation Center.

Behavioral Setup. All tasks were performed with EGS seated in his motorized wheel chair. Tasks involved the use of an anthropomorphic robotic limb, a 47 in. LCD monitor, or a combination of both. The robotic limb was bolted to a steel frame positioned in front of and offset to the right of the subject's chair with the shoulder mount at approximately eye level. The arm was always positioned 48 inches from the subject's body to maintain a safety zone. When the robotic limb was not needed for the task, it was moved outside the subject's field of view. The LCD monitor was positioned approximately 184 cms from the subject's eyes. Stimulus presentation was controlled using the Psychophysics Toolbox (23) for MATLAB.

We used the Modular Prosthetic Limb (MPL), a robotic arm designed through the Johns Hopkins University (JHU) Applied Physics Laboratory (APL). It was designed to approximate the function of a human arm, and its size and ranges of motion were specified to match those of a human arm as closely as possible. The MPL has 17 degrees of freedom, and, fully extended, the MPL is approximately 79 cm long. During prosthetic control, the full set of degrees of freedom were constrained to either 2d or 3d control of the position of the hand. In some tasks, EGS was required to use the MPL to point to targets displayed on the LCD display. A manual calibration session was used to register the coordinate frames of the display and MPL for these sessions.

Neural Recordings. EGS was implanted with two 96-channel Neuroport arrays in putative homologues of area AIP and Brodmann's Area 5d (Fig. S1B). Neural activity was amplified, digitized, and recorded at 30KHz with the Neuroport neural signal processor (NSP) (Fig. 2). The Neuroport System, comprising the arrays and NSP, has received FDA clearance for <30 days acute recordings; for purposes of this study we received FDA IDE clearance (IDE #G120096) for extending the duration of the implant.

For online prosthetic control, we used the time of unsorted action potential threshold crossings. In the Central software suite, thresholds for action potential detection were set at -4.5 times the root-mean-square of the high-pass filtered (250Hz cut-off) full-bandwidth signal. The time of threshold crossings were transmitted in real-time to MATLAB, counted in non-overlapping 50ms time bins, and utilized by the decoding algorithm to drive the prosthetic device. For online prosthetic control, a minimum firing rate of 2 Hz was enforced. For offline analysis, single and multiunit activity was sorted using Gaussian mixture modeling of the 2d principal component projection of waveforms detected via threshold crossing.

Task Descriptions. The purpose of the clinical study was to understand the relationship between neural activity recorded in human PPC as it relates to imagined movement of the arm and hand, and the utility of these signals for prosthetic control. To this end, we utilized a variety of experimental paradigms, some designed to help characterize the nature of PPC tuning while accounting for possible confounds, and some designed to provide a simplified test bed for prosthetic control.

Functional imaging task. Following an initial fixation phase, the subject was cued to the type of imagined action to perform (precision grip, power grip, or reach without hand shaping) (Fig. S1A). An object was then presented. If the object was "whole", the subject performed the cued action ("Go" condition.) If the object was "broken," the subject withheld the imagined movement ("NoGo" condition). In the example provided, the subject would imagine reaching out toward and precision gripping the narrow part of the object. The orientation of the object was pseudo-randomly selected from one of 6 possible orientations and the subject was allowed to freely choose whether they reached for the object using an overhand or underhand posture. During fMRI training sessions, the subject was instructed to report the color of the portion of the object closest to their thumb allowing us to infer whether the subject reached with an overhand or underhand posture. Behavioral analysis verified that EGS chose arm postures that followed biomechanical constraints suggesting an ability to imagine naturalistic arm movements (24).

Biofeedback. The biofeedback tasks were performed in a freeform manner. EGS was shown a panel that provided basic visual feedback on the firing rate of an isolated single neuron while also listening to the broadband activity from the same channel (Movie S1, S2). The experimenter and EGS then worked together to determine the type of imagined action that best modulated neural activity. In some cases this involved the experimenter instructing EGS to imagine a variety of actions, in other cases, EGS was instructed to "play" with the neuron, trying different actions on his own to see if he could find the action that evoked or suppressed activity. If a unit seemed well tuned to a particular action, EGS was verbally cued to imagine said action along with a variety of similar and dissimilar actions to test the relative specificity of the unit to the action (Movie S1).

Masked Memory Reach. The masked memory reach task was used to quantify goal and trajectory tuning in PPC while controlling for visual confounds related to target placement and visual motion of the cursor (Fig. 1A). Following an inter-trial interval, a spatial cue was flashed at one of 4 spatial locations equally spaced along a circle centered at the fixation point. At the same time, the effector (a circular cursor) was presented at the point of fixation. The cursor was held at this location until after the go cue. Sustained activity during the delay period was used to test for neural encoding of the goal of the movement. Following the delay period in which no target was visible, all possible targets appeared simultaneously to ensure that spatial tuning following the go cue could not be attributed to visual transients. In the open-loop condition, following a 250 ms delay, the cursor would move automatically to the cued target with an approximately bell-shaped velocity profile. In the closed-loop condition, following a 250 ms delay, control of the cursor was passed to the subject, and the subject, under neural control, would move the cursor to the target. Transient spatially tuned activity during the movement period was used to test for neural encoding of the trajectory. We tested trajectory tuning under two conditions. In one condition, the subject could clearly see movement of the cursor. In the

second condition, an annulus was used to mask motion of the cursor from its initial starting location to the inner edge of the target.

Point-to-Point. The point-to-point task provided a simple environment that allowed EGS to test his ability to spatially position a prosthetic effector. Under free gaze, targets were presented one at a time on the LCD display. During open-loop decoder calibration sessions, following a 250 ms delay relative to target onset, the effector would move automatically to the cued target with an approximately bell-shaped velocity profile. In the closed-loop condition, EGS guided the neurally controlled effector to the target (Movie S3). A trial was considered successful if EGS was able to maintain the position of the effector over the target for 1s. During some sessions, a simple cursor, rendered on the display, was used as the effector. During other sessions, EGS used the MPL, constrained to move in a 2D plane, to point to the targets that appeared on the monitor. Sometimes both the MPL and cursor were shown simultaneously.

Goal Selection Task. The goal selection task provided a simple environment for testing the ability to directly select spatial targets in closed-loop (Fig. 3A). Following an inter-trial interval, a fixation cue was presented at the center of the screen. In addition to fixating the cue, EGS was instructed to imagine his right arm pointing at the fixation cue. The location of a spatial goal was then flashed at one of six pseudo-randomly chosen peripheral locations. EGS was instructed to intend a right arm reach to the cued location. During calibration runs, data from the final 500 ms of the delay period was used to train a classification algorithm. During brain control runs, data from the final 500ms of the delay period was used to decode the location of the spatial target. Dependent on the relative location of the decoded and veridical target location, EGS was awarded points. Following display of the awarded point total, the location of the decoded target location was presented.

Symbolic Cue Task. The symbolic cue task provided a means of testing the response properties of the neural population without the presence of visual transients at the cued target locations (Fig. 3B). The task was structured as follows: Following an inter-trial interval, a target grid was presented on the monitor. In addition to fixating the center target, EGS was instructed to imagine his right or left arm pointing to the center target during reach trials, or simply looked at the center target for saccade trials. The location of a spatial goal was then indicated by a number presented at the point of fixation. The numeric cue was removed during a delay period. After the delay, a beep indicated that EGS should initiate an imagined movement toward the cued location. A second beep (1s after the initiation beep) was used to cue EGS when the movement should have ended in an effort to stereotype the imagined movement. Approximately 15% of trials were Catch trials. During Catch trials, a distinct beep randomly chosen between .2 and .8 seconds after movement initiation was followed by presentation of letters arrayed between the center and peripheral targets. EGS reported the approximate position of his hand by verbally indicating the character closest to the position of his imagined hand. This provided a means to ensure that EGS was, on average, engaged in the task by checking whether the reported letter was consistent with the cued target, and allowed us to verify the approximate timing of his reach trajectories as the reported letter was an approximate measure of movement distance.

Neuroimaging. Functional imaging was performed at the USC Keck Medical Center using a GE 3T scanner with an 8-channel head-coil. Functional data was acquired using T2*-weighted single-shot echo-planar acquisition sequence (TR = 2000 ms; slice thickness = 3 mm; in-plane resolution = 3 x 3 mm; TE = 30 ms; flip angle = 80; fov= 192 x 192 mm; matrix size = 64 x 64; 33 slices (no-gap) oriented 20 degrees relative to ACPC line). The anatomical was

acquired using the GE T1 Bravo sequence (TR = 1590 ms; TE = 2.7 ms; fov =176 x 256 x 256 mm; 1 mm isotropic voxels).

General linear model (GLM) analysis was performed using Analysis of Functional NeuroImages (AFNI) (25). Functional runs were slice scan-time corrected, 3D motion corrected, spatially smoothed (3mm full-width half-max), masked to only include voxels within the superior parietal lobule, converted to percent signal change, and detrended. Regressors aligned to stimulus onset were generated with AFNI's BLOCK function with two second duration to model the expected hemodynamic response. Motion correction parameters were included in the regression model. Significance was determined at a false discovery rate (FDR) q of 0.05. Freesurfer (http://surfer.nmr.mgh.harvard.edu/) was used for cortical surface reconstructions. Regressors of interest included "Reach-Go", "Reach-NoGo", "Grasp-Go", and "Grasp-NoGo". Reach-related areas were identified by the contrast "Reach-Go">"Reach-NoGo." Grasp related areas were defined by the conjunction of contrasts "Grasp-Go">"Grasp-NoGo" and "Grasp-Go">"Reach-Go."

Discrete Classification. Classification was performed using linear discriminate analysis. The classifier took as input a vector comprised of the number of spikes occurring within a specified time epoch for each recording channel (for online use) or sorted unit (for offline analysis). The following assumptions were made for the classification model: one, the prior probability across the classes was uniform, two, the conditional probability distribution of each feature on any given class was normal, three, only the mean firing rates differ for each class (the covariance of the normal distributions were the same for each class), and, four, the firing rates of each input are independent (covariance of the normal distribution was diagonal). Reported performance accuracy was based on leave-one out cross-validation. Features that demonstrated non-significant tuning based on a preliminary ANOVA test were excluded from the input vector to reduce the total number of features. For purposes of cross-validation, the ANOVA test exclusion criteria was calculated on the training set and applied to the test set to avoid "peaking" affects.

Classification accuracy through time. To compute the temporal dynamics of classification accuracy, the neural data was first aligned to a behavioral epoch (e.g. cue onset). Spike counts were then computed in 300ms windows spaced at 10 ms intervals. The 300ms window was chosen to balance the need to have a sufficient spike count within the window to allow accurate decoding while being short enough to see how the dynamics of decode accuracy evolved in time.

For offline goal decoding analysis, trials from the open-loop (training) and closed-loop (brain control) conditions were combined in order to increase the total number of trials and therefore improve model estimation when constructing the classifier. This approach is reasonable given that task requirements and visual feedback were identical during the cue and delay period of the tasks for the open and closed loop sessions. Analysis was performed on open-loop and closed-loop sessions separately and resulted in qualitatively similar results. Comparison of open-loop and closed-loop responses, and the implication for decoder calibration methods, will be addressed in future work.

Trajectory Decoding. The instantaneous velocity of the cursor in the MMR task was reconstructed using the movement portion of each trial plus a 500 ms window surrounding the movement period (when cursor velocity was zero). Data taken before and after movement were included to ensure that the decoder training data captured periods when EGS intended to remain

stationary as well as periods when EGS intended to move. In constructing the decoder, we collapsed across the masked and unmasked trials. This both increased the total number of trials that were used for calibration and ensured that the resulting performance measure reflected the ability to generalize across the two contexts.

Trajectories were reconstructed using a L1-constrained linear least squares regression (lasso) between smoothed neural features binned into 50ms windows and cursor velocity after identifying an optimized lag. Neural data was smoothed by convolving an 800 ms duration minimum jerk velocity profile with the neural response. Lags were tested in the range of 300 ms and 0 ms, in 100 ms intervals, with neural features preceding kinematics. Similar to classification analysis, features that demonstrated non-significant tuning based on a preliminary per-unit regression analysis were excluded from trajectory reconstructions. This was done to minimize the likelihood of over-fitting training data which in turn would lead to poor generalization as measured by cross-validation. Importantly, in the cross-validation analysis, the feature selection criteria was calculated on the training set and applied to the test set to avoid "peaking" effects artificially inflating cross-validated R^2 estimates.

Our trajectory analysis for the neuron dropping curves combined the activity of units across days. For reconstruction of trajectory, data was collected from the open-loop/decoder training session of the MMR task (Fig. 1A). The open-loop session was used because, for a given target, the kinematic response of the effector was the same regardless of the day, allowing different neurons' firing activities from different days to be fitted to the same kinematic output.

Neuron Dropping Curves. To construct the greedy neuron-dropping curves of Fig. 2 B&D and Fig. 3D, a greedy algorithm was used in which features were added one at a time to the growing pool of features based on the relevant performance measure (cross-validated accuracy for discrete classification; cross-validated R^2 for continuous decoding). In the first iteration, each feature was processed independently to derive the performance measure. The feature with the highest measure was removed from the pool of available features and placed in the pool of used features. Next, each of the remaining features was combined with the previously selected feature, and a second feature was selected. This process – combining each available feature with the used-feature set, constructing a decoder, and moving the feature corresponding to the highest measure from the available to the used list – was repeated until the available feature list was empty. The performance saturation point of the greedy curve represents the optimal subset of features that should be used to optimize generalization performance. The inclusion of additional features decreases generalization performance by over-fitting training data, a phenomena known to hurt online control (26).

Random neuron-dropping curves were constructed to test expected performance as a function of the size of the recorded neural population. To construct the random neuron-dropping curves of Fig. 3C and Fig. S3, we computed cross-validated decode accuracy (classification) or cross-validated R^2 (trajectory reconstruction) for test populations of neurons ranging in size from 1 to 100 units. Each test population was generated by randomly sub-selecting, without replacement, the specified number of units from the entire ensemble of recorded units. For each population size, units were randomly drawn and cross-validated accuracy was computed 100 times to allow estimation of the variability in accuracy. As discussed in the "Discrete classification" and "Trajectory decoding" sections above, we included feature selection as part of

the decoder calibration process. As a result, the actual decoding algorithm was trained on a subset of the total number of units as determined by a per-unit significance test calculated on the training data (not including the test data) used for cross-validation analysis.

Combining data across days. Our offline decoding analysis relied on combining data across days. All offline decoding analysis was performed using sorted units. Sorted units were retained for analysis only if they included at least 8 trials per target and met a minimum firing rate of 2Hz. Each session's neural data was sorted independently, and neurons present on the same channel were assumed to be different if they appeared on different days (i.e., no attempt was made to equate a neuron on day 1 with a neuron on day 2 – they were assumed to be different neurons). This was driven by the fact that waveforms changed from day to day and methods to determine whether waveforms resulted from the same unit tended to indicate that units were independent (see also Fig. S2).

We used the following scheme for combining neurons across days: An "observation" of a given trial type (e.g. movement to the right) was created by randomly sampling without replacement, the activity of each unit in the recorded population of the same trial type, regardless of the day. By repeating this process, a synthetic dataset composed of observations that included units recorded on separate days was generated. Importantly, because this process was done without replacement, no two observations in the synthetic dataset contained the same data, thus preventing potential "twinning" effects in our cross-validation analysis.

Goal versus trajectory analysis. The masked memory reach task (Fig. 1A) was used to determine whether units were goal-tuned, trajectory-tuned, or both. Analysis to determine a unit's preference was performed as follows. For units that exceeded a minimum firing rate of 2 Hz, a multiple linear regression model was constructed that explained each unit's firing rate as a function of an initial visual transient, a sustained goal response, and a transient representation of movement velocity (Fig. 1B). The transient activations were modeled as minimum jerk velocity profiles (similar in shape to a truncated Gaussian) of 500 and 750 ms duration for the visual and trajectory components, each starting at the beginning of their respective phases. The goal related activity was modeled as a smoothed step function rising 250ms after cue onset, peaking around 500ms after cue onset, and sustaining its peak value through the movement period. The potential for maintaining the representation of the goal through the movement period forms the basis for why the analysis was done as described in contrast to e.g. picking non-overlapping temporal epochs during the cue, delay, and go periods and checking for spatial tuning. By allowing a model with overlapping temporal representations we were able to partial out the variance attributable to each component.

The regression resulted in a set of beta coefficients along with associated p-values for each of these possible components. The reported results were restricted to units exhibiting significant tuning to at least goal or trajectory. To determine tuning, the p-values associated with trajectory and goal were tested for significance using the Holm-Bonferroni method to correct for multiple comparisons (N=698; 2 parameters per unit, 349 units). 124 units had a significant beta coefficient for either trajectory or goal. The significance of the beta values of these units was then used to classify each unit. 24 of 124 units were significant for the goal component but not the trajectory component, 67 of 124 units were significant for the trajectory component but not the goal component. 33 of 124 units were significant for both goal and trajectory.

Effector specificity. Effector specificity was tested in the context of the symbolic cue task (Fig. 4B). Effectors were tested in interleaved blocks of 6 repetitions to each target. Target order was randomized within a block. Two or three blocks per effector and two or three effectors were tested during each session. Neural data was analyzed using the average neural response between 200 and 800 ms following the go cue as this epoch showed the largest directionally tuned response.

The degree to which neural activity showed a preference for an effector was quantified using an effector specificity index (ESI) based on the relative depth of modulation (DM) for each effector:

$$\left(ESI = \frac{DM_{effector1} - DM_{effector2}}{DM_{effector1} + DM_{effector2}}\right)$$

DM was defined as the difference between the mean firing rate for movements in the preferred direction (the direction evoking maximum neural activation) and the anti-preferred direction (the direction opposite the preferred direction.) ESI is a value ranging between 1 and -1. An ESI of 1 indicates exclusive tuning to effector 1, an ESI of -1 indicates exclusive tuning to effector 2, and an ESI of 0 indicates that the tuning, as measured by DM, is identical between the two effectors. ESI was only computed for units with a significant DM for at least one effector as determine by a t-test between the evoked neural response to the preferred and anti-preferred directions. We used a shuffle test to determine if differences in DM were significant. A veridical estimate of the difference in DM was computed between effectors (i.e. $DM_{effector1} - DM_{effector2}$). An empirical null distribution was then computed by randomly assigning trials to each effector and recomputing the difference in DM. This shuffle procedure was repeated 10000 times. A p-value was generated using a rank test, e.g. by counting the number of shuffles greater than or less than the veridical estimate.

To decode whether EGS made a saccade or imagined a right arm movement or imagined a right arm or left arm movement (Fig. 4F) we used the following procedure: First, the positional tuning of each unit was regressed out by subtracting the mean neural response for each target regardless of effector. The resulting residual responses for each unit were than subjected to boot-strapped cross-validated classification of effector type. Each day was analyzed independently and the mean classification accuracy and mean confidence intervals are displayed (Fig. 4F).

Whereas M1 neurons are primarily active for movements of the contralateral limb, PPC neurons have activity related to both the contralateral and ipsilateral limbs. Furthermore, we have shown that individual neurons in PPC can selectively code movements of the (contralateral) limb or left (ipsilateral) limb. The population response allowed us to decode which of the two effectors EGS imagined moving. These results suggest the possibility of independently controlling two robotic limbs with recordings made from one hemisphere. Many neurons showed comparable activity to either effector and thus may not be useful for independent control. One possibility is that these units could be used for coordinating the motion of two arms by providing an information pathway that chains motion of one arm to the other. The importance of both independent and coordinated control can be illustrated in a simple example of

pouring coffee into a mug. When pouring, independence of control is needed as one limb must hold the cup steady while the other performs a pouring motion. Coordination is also needed to ensure that movement of one limb is compensated for by the other limb, e.g. if the hand holding the mug is moved, the pouring hand must also be moved to prevent coffee from being spilled onto the floor. Given the true complexity inherent in controlling two limbs across the spectrum of human behavior, future work demonstrating the ability to perform coordinated and independent motion of both limbs simultaneously will be necessary in order to fully test the potential for controlling two limbs from PPC.

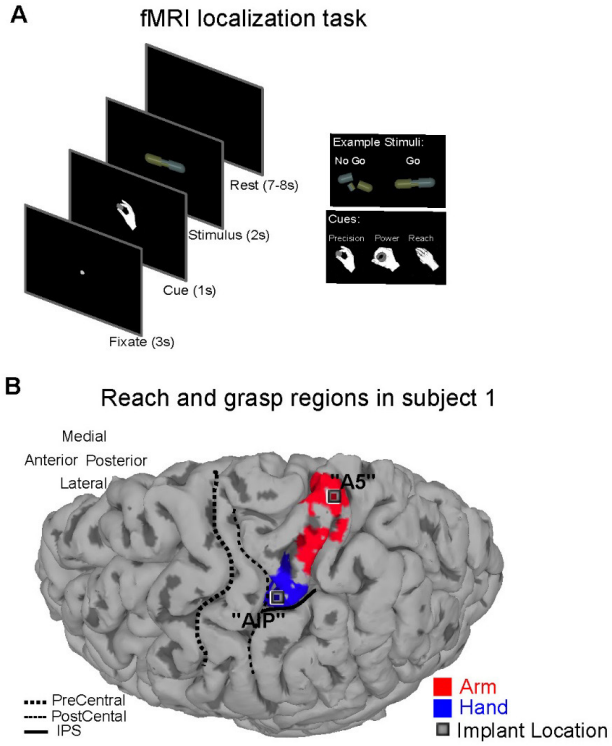

Fig. S1. Functional Localization of Implant Sites. Functional magnetic resonance imaging was used to identify candidate implant sites based on the BOLD response to imagined reaching and grasping actions. (A) Task design. Following an initial fixation phase, the subject was cued to the type of imagined action to perform (precision grip, power grip, or reach without hand shaping). An object was then presented. If the object was "whole", the subject was instructed to imagine performing the cued action ("Go" condition.) If the object was "broken," the subject withheld the imagined movement ("NoGo" condition). The orientation of the object was pseudo-randomly selected from one of 6 possible orientations and the subject was allowed to freely choose whether they reached for the object using an overhand or underhand posture. Behavioral analysis of choice preferences of arm posture verified that EGS chose arm postures that followed biomechanical constraints suggesting an ability to imagine naturalistic arm movements. (B) Functional results rendered on a reconstructed cortical surface. Areas with significantly greater activation for the Reach "Go" condition as compared to the "No-Go" condition are shown in Red. Areas showing greater activation for the Grasping "Go" condition compared to the "No-Go" condition and showing greater activation for the Grasping "Go" condition compared to the Reach "Go" condition are shown in blue. Statistical analysis was restricted to the superior parietal lobule to increase statistical power. Implant sites as shown (Talairach coordinates: AIP = [-38 lateral, -53 posterior, 46 superior], BA5 = [-18 lateral , -68 posterior, 48 superior]).

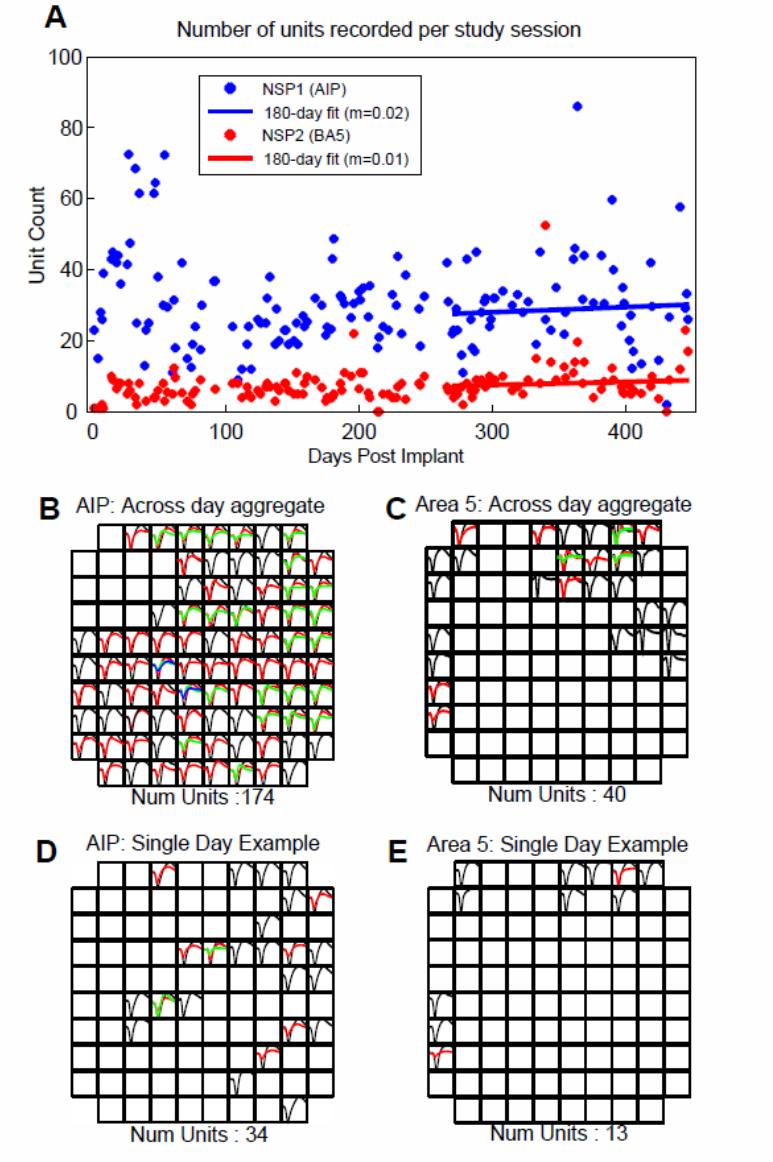

Fig. S2. Neural recordings. A. The quality of neural recordings varied substantially day-to-day with as few as 13 units to as many as 105 units recorded across the two arrays. Greater than 90% of sessions resulted in a total neural yield between 20 and 50 sorted units. B-E. The electrodes on which neural activity was recorded varied day-to-day resulting in our ability to sample the activity of a large population of neurons across sessions. To illustrate, a composite array that plots sorted waveforms at their respective electrode positions on the recording array is shown (B,C). The composite array was constructed by independently checking the number of waveforms at each electrode for each study session, and plotting the waveforms for the study session that contained the greatest number of differentiable units at the electrode. This provides a lower bound on the total number of independent units that were tested on each array (174 for AIP and 40 for Area 5). D&E shows an example of the neural yield recorded during a single study session.

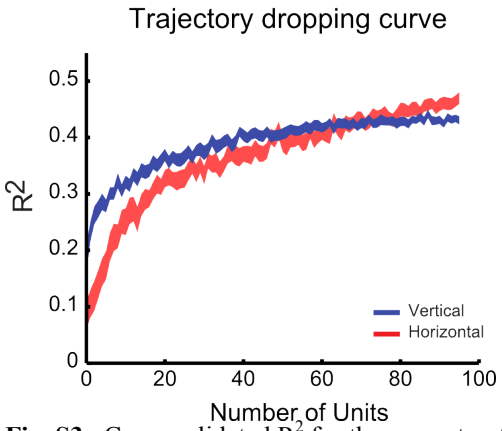

Fig. S3. Cross-validated R^2 for the reconstruction of instantaneous velocity of the cursor in the MMR task (mean with 95% confidence interval) for variable neural population sizes. Populations were constructed using units randomly sampled from the ensemble of recorded units with data taken from the movement period of the task plus a 500 ms window surrounding the movement period (when cursor velocity was zero).

Movies S1-S3

Movie S1. Encoding of high-level behaviorally meaningful actions in human PPC. Example biofeedback session illustrating the activity of a single neuron that shows selectivity for imagined movement of either hand to the mouth. Movements with similar gross properties such as movement of the hand to the ear evoke a minimal response. Units tuned to behaviorally meaningful high-level intentions could be used to command a smart robotic limb to e.g. bring the hand to the mouth for purposes of self-feeding without the need to control the moment-to-moment position of the limb.

Movie S2. Example biofeedback session illustrating the ability of the subject to control the activity of a single unit using imagined actions. EGS was able to evoke robust activity in this unit by imagining rotation of his right shoulder. EGS was able to silence the unit by imagining movement of his hand to his nose.

Movie S3. Example of continuous neural control of the robotic limb in two dimensions.

References and Notes

1. R. A. Andersen, C. A. Buneo, Intentional maps in posterior parietal cortex. *Annu. Rev. Neurosci.* **25**, 189–220 (2002). Medline doi:10.1146/annurev.neuro.25.112701.142922

2. J. C. Culham, C. Cavina-Pratesi, A. Singhal, The role of parietal cortex in visuomotor control: What have we learned from neuroimaging? *Neuropsychologia* **44**, 2668–2684 (2006). Medline doi:10.1016/j.neuropsychologia.2005.11.003

3. R. Balint, Seelenlahmung des "Schauens," optische Ataxie, raumliche Storung der Aufmerksamkeit. *Monatsschr. Psychiatr. Neurol.* **25**, 51–81 (1909).

4. M. T. Perenin, A. Vighetto, Optic ataxia: A specific disruption in visuomotor mechanisms. I. Different aspects of the deficit in reaching for objects. *Brain* **111**, 643–674 (1988). Medline doi:10.1093/brain/111.3.643

5. M. A. Goodale, A. D. Milner, Separate visual pathways for perception and action. *Trends Neurosci.* **15**, 20–25 (1992). Medline doi:10.1016/0166-2236(92)90344-8

6. A. Sirigu, J. R. Duhamel, L. Cohen, B. Pillon, B. Dubois, Y. Agid, The mental representation of hand movements after parietal cortex damage. *Science* **273**, 1564–1568 (1996). Medline doi:10.1126/science.273.5281.1564

7. L. Pisella, H. Gréa, C. Tilikete, A. Vighetto, M. Desmurget, G. Rode, D. Boisson, Y. Rossetti, An 'automatic pilot' for the hand in human posterior parietal cortex: Toward reinterpreting optic ataxia. *Nat. Neurosci.* **3**, 729–736 (2000). Medline doi:10.1038/76694

8. S. Musallam, B. D. Corneil, B. Greger, H. Scherberger, R. A. Andersen, Cognitive control signals for neural prosthetics. *Science* **305**, 258–262 (2004). Medline doi:10.1126/science.1097938

9. M. Hauschild, G. H. Mulliken, I. Fineman, G. E. Loeb, R. A. Andersen, Cognitive signals for brain-machine interfaces in posterior parietal cortex include continuous 3D trajectory commands. *Proc. Natl. Acad. Sci. U.S.A.* **109**, 17075–17080 (2012). Medline doi:10.1073/pnas.1215092109

10. G. H. Mulliken, S. Musallam, R. A. Andersen, Decoding trajectories from posterior parietal cortex ensembles. *J. Neurosci.* **28**, 12913–12926 (2008). Medline doi:10.1523/JNEUROSCI.1463-08.2008

11. R. A. Andersen, S. Kellis, C. Klaes, T. Aflalo, Toward more versatile and intuitive cortical brain-machine interfaces. *Curr. Biol.* **24**, R885–R897 (2014). Medline doi:10.1016/j.cub.2014.07.068

12. W. Truccolo, G. M. Friehs, J. P. Donoghue, L. R. Hochberg, Primary motor cortex tuning to intended movement kinematics in humans with tetraplegia. *J. Neurosci.* **28**, 1163–1178 (2008). Medline doi:10.1523/JNEUROSCI.4415-07.2008

13. S.-P. Kim, J. D. Simeral, L. R. Hochberg, J. P. Donoghue, M. J. Black, Neural control of computer cursor velocity by decoding motor cortical spiking activity in humans with tetraplegia. *J. Neural Eng.* **5**, 455–476 (2008). Medline doi:10.1088/1741-2560/5/4/010

14. J. W. Gnadt, R. A. Andersen, Memory related motor planning activity in posterior parietal cortex of macaque. *Exp. Brain Res.* **70**, 216–220 (1988). Medline

15. G. H. Mulliken, S. Musallam, R. A. Andersen, Forward estimation of movement state in posterior parietal cortex. *Proc. Natl. Acad. Sci. U.S.A.* **105**, 8170–8177 (2008). Medline doi:10.1073/pnas.0802602105

16. D. M. Wolpert, S. J. Goodbody, M. Husain, Maintaining internal representations: The role of the human superior parietal lobe. *Nat. Neurosci.* **1**, 529–533 (1998). Medline doi:10.1038/2245

17. L. H. Snyder, A. P. Batista, R. A. Andersen, Coding of intention in the posterior parietal cortex. *Nature* **386**, 167–170 (1997). Medline doi:10.1038/386167a0

18. S. W. C. Chang, A. R. Dickinson, L. H. Snyder, Limb-specific representation for reaching in the posterior parietal cortex. *J. Neurosci.* **28**, 6128–6140 (2008). Medline doi:10.1523/JNEUROSCI.1442-08.2008

19. S. Dangi, S. Gowda, H. G. Moorman, A. L. Orsborn, K. So, M. Shanechi, J. M. Carmena, Continuous closed-loop decoder adaptation with a recursive maximum likelihood algorithm allows for rapid performance acquisition in brain-machine interfaces. *Neural Comput.* **26**, 1811–1839 (2014). Medline doi:10.1162/NECO_a_00632

20. A. P. Georgopoulos, J. F. Kalaska, R. Caminiti, J. T. Massey, On the relations between the direction of two-dimensional arm movements and cell discharge in primate motor cortex. *J. Neurosci.* **2**, 1527–1537 (1982). Medline

21. L. R. Hochberg, M. D. Serruya, G. M. Friehs, J. A. Mukand, M. Saleh, A. H. Caplan, A. Branner, D. Chen, R. D. Penn, J. P. Donoghue, Neuronal ensemble control of prosthetic devices by a human with tetraplegia. *Nature* **442**, 164–171 (2006). Medline doi:10.1038/nature04970

22. J. L. Collinger, B. Wodlinger, J. E. Downey, W. Wang, E. C. Tyler-Kabara, D. J. Weber, A. J. McMorland, M. Velliste, M. L. Boninger, A. B. Schwartz, High-performance neuroprosthetic control by an individual with tetraplegia. *Lancet* **381**, 557–564 (2013). Medline doi:10.1016/S0140-6736(12)61816-9

23. D. H. Brainard, The Psychophysics Toolbox. *Spat. Vis.* **10**, 433–436 (1997). Medline doi:10.1163/156856897X00357

24. K. L. Macuga, S. H. Frey, Neural representations involved in observed, imagined, and imitated actions are dissociable and hierarchically organized. *Neuroimage* **59**, 2798–2807 (2012). Medline doi:10.1016/j.neuroimage.2011.09.083

25. R. W. Cox, AFNI: Software for analysis and visualization of functional magnetic resonance neuroimages. *Comput. Biomed. Res.* **29**, 162–173 (1996). Medline doi:10.1006/cbmr.1996.0014

26. S. M. Chase, A. B. Schwartz, R. E. Kass, Bias, optimal linear estimation, and the differences between open-loop simulation and closed-loop performance of spiking-based brain-computer interface algorithms. *Neural Netw.* **22**, 1203–1213 (2009). Medline doi:10.1016/j.neunet.2009.05.005